X-Band Noise Temperature Near the Sun at a 34-Meter High Efficiency Antenna

T. A. Rebold and T. K. Peng
Telecommunications Systems Section

S. D. Slobin
Radio Frequency and Microwave Subsystems Section

X-band system noise temperature near the sun was measured at DSS 15, a 34-meter High Efficiency (HEF) antenna, in November 1987. Data was taken at angles off the center of the sun from 0 to 4 degrees. At angles greater than 0.5 degree, the measured results agree with Voyager tracking data taken at Solar Conjunction in late December 1987. Within the solar disk, at angles lower than 0.27 degree, the temperature measured was lower than the prediction of a model by 30 percent, after adjusting for known receiver nonlinearities. The discrepancy in this extreme case is probably caused by unknown nonlinearities in the receiver, uncertainties in the model, or both. The measurement is nevertheless credible for practically all Sun–Earth–Probe angles of interest to deep space missions.

I. Introduction

On November 26 and 27 of 1987, a test was performed at DSS 15 to determine the effect of solar radiation on the system noise temperature at low Sun–Earth–Probe (SEP) angles. This test was prompted by the need to gather data in preparation for an advanced receiver test scheduled one month later during the Voyager solar conjunction, a low SEP angle event.

Existing data on solar noise effects given in the *DSN/Flight Project Interface Design Handbook*[1] is insufficient on two counts. First, data provided pertains only to the 64-m antenna and not to the newer High Efficiency (HEF) antenna at DSS 15. Second, this 64-m data does not identify the solar radiation level, which varies widely at X-band throughout the 11-year cycle of sunspot activity.

Previous solar noise temperature measurements carried out at JPL include those at 2297 MHz measured at the DSS 14 64-m antenna [1] and at 20.7 GHz and 31.4 GHz, made with an early-model DSN water vapor radiometer [2]. No such measurement at X-band has been performed. Therefore, an additional factor motivating this measurement was to provide data necessary to characterize the HEF antenna performance in the design handbook.

The measured data was compared with two additional sources of information. The first source is a prediction from an

[1] *DSN/Flight Project Interface Design Handbook*, JPL Document 810-5 (internal report), vol. 1, module TCI-40, Jet Propulsion Laboratory, Pasadena, California, 1983.

analytical model of a large dish antenna taking into account the solar flux measurements for November 26 and 27 provided by the National Oceanic and Atmospheric Administration (NOAA). The second source is an independent noise temperature measurement obtained from DSS 43 and DSS 15 one month later during the Voyager solar conjunction. This measurement was taken using the regular station Noise Adding Radiometer (NAR).

The report is divided into three major parts. Section II describes the measurement and the data taken. Section III describes an analytical model used to predict the system noise temperature when the antenna is pointing directly on the sun. Finally, Sections IV and V conclude the report by comparing the measured data with the prediction and with the Voyager observations. Error analysis for the measurement is presented in the Appendix.

II. Measurement

A. Observation Strategy

A total of 5 hours over two days was allocated to the performance of the measurement at the station, allowing the sampling of about 100 points on two quadrants of the plane perpendicular to the boresight of the antenna. Since the sun was anticipated to pass above the probe during the conjunction, the top two quadrants were chosen for the measurement. The points were picked to lie on a Cartesian grid indexed by the sun's elevation and cross-elevation offsets from the probe.

An existing contour map showing the gain distribution of DSS-13, a 26-meter antenna with a similar quadripod structure supporting the antenna subreflector, was used as a guide for the selection of data points. This map showed that significantly higher sidelobes are generated by the antenna quadripod structure. In order to investigate the effects of the quadripod structure on solar noise temperature increases, a large number of points were chosen to lie along these sidelobes, which form two diagonals crossing the origin at 45 and 135 degrees.

At the station, the Antenna Pointing Assembly (APA) was given the coordinates of the sun for tracking in planetary mode, as well as a list of the desired sample points converted beforehand into elevation and azimuth offsets from the sun. The sample points were compiled into a series of command macros and input into the APA by the station operator. On both days the measurements were made in late afternoon, when the elevation of the sun varied from about 24 to 7 degrees. Correspondingly, the antenna efficiency varied from about 64 percent to 61 percent due to gravity-induced structural deformations.

B. Instrumentation

A block diagram of the station configuration and the instrumentation used to perform the test is shown in Fig. 1. Data was recorded using a "quasar meter" being developed by the DSN Operations for use in VLBI applications. The quasar meter consists of an HP 9816 computer recording power measurements from an HP 436A power meter, which is connected to the 300-MHz IF distribution of the open-loop receiver. The station was receiving in X-band using the Block II maser. The Y-factor machine connected to the Block III closed-loop receiver was used to provide pre-, post-, and in-track system temperature calibrations. It also served as a real time monitor of the noise power received during the measurement.

C. Measurement Procedures

Prior to tracking, station personnel performed a precalibration by recording ambient load and cold sky noise levels with the quasar meter and measuring the associated system temperatures with the standard DSN Y-factor method. During tracking mode, data was recorded at a rate of one sample per second, while the antenna was pointed at the various elevation and cross-elevation offsets from the sun. The typical dwell time at a given point was 2.5 minutes, except for occasional sweeps across the origin (sun) with dwell times at 20 seconds per point. The ambient load was switched in periodically to ascertain proper functioning of the test configuration. After tracking, a final postcalibration was performed.

D. Data Analysis

Several steps were required to turn the raw power samples into system noise temperature measurements. First, the average and standard deviation of the power samples acquired at each antenna offset were computed. Second, the power measurements were converted into noise temperature using the pre- and post-calibrations. The third step involves normalizing the temperatures to zenith by subtracting out the system noise temperature as a function of elevation angle (see Fig. 2, which was the result of a separate measurement). The resulting temperatures indicate system noise level increases due to the presence of the sun at particular offsets from the antenna boresight. This temperature will be referred to as the Solar Noise Temperature (T_{sn}).

For very high noise temperatures, an additional step is taken to adjust for the effect of saturation in the receiving system. To estimate the saturation effect, the gains and bandwidths of the amplifiers in Fig. 1 are given in Fig. 3. Gain compression occurs in the maser or in the RF/IF converter when the output power of either amplifier reaches its own saturation level. Data on the Block IIA maser, which has the same saturation characteristics as the Block II maser used in this measure-

ment, indicates significant saturation above 2900 kelvins as seen in Table 1 (data provided by S. Petty, Radio Frequency and Microwave Subsystems Section). Note that this data refers to the noise power at the input of the maser which was tuned to 45-dB gain. Data on the RF/IF converter (provided by M. Lambros of the same section) indicates a 1-dB compression level at 26 dBm and 0.1-dB compression at 16 dBm measured at the output of the converter, using a sinusoidal test signal.

A quadratic curve fitted to the first three points of Table 1 was applied to the power measurements from the quasar meter in order to compensate for the maser compression. The maximum adjustment was about 0.3 dB for power readings taken with the antenna pointed at the sun's center. At this location, the adjusted T_{sn} reached its maximum of 8240 kelvins.

This level of solar noise will not saturate the RF/IF converter according to the overall gain and bandwidth as shown in Fig. 3. With a total gain of 85 dB from maser to converter and an effective bandwidth of 100 MHz, the output level from the RF/IF converter will reach only about 5.6 dBm at the maximum system noise temperature. This is still about 10 dB lower than the 0.1-dB compression point of the converter (16 dBm).

However, there are uncertainties in the measurement of gain compression (about 0.1 dB), and the measured equipment was typical and not the actual equipment at DSS 15. Thus the error in the nonlinearity compensation applied to the power measurements could be as high as 10 percent in the positive direction due to the possibility of additional sources of compression. Since it is more likely that there will only be more nonlinearity than what was measured and not less, the error in the negative direction should be less than 2 percent. This assumption on the error in the nonlinearity compensation will be used in the error analysis in the appendix.

Figures 4 and 5 show two quadrants of the antenna's field of view in the elevation versus cross-elevation coordinate system. The locations where noise temperature was measured are indicated by black dots. They are accompanied by the measured solar noise temperature T_{sn}.

Figure 6 shows the entire data set condensed into a plot of solar noise temperature versus SEP angle. The points are divided into two categories: those that lie along the quadripod sidelobes at 45 and 135 degrees and those that do not. As seen in the figure, for a given SEP angle the sun's influence on the system noise temperature is greater if it lies along a quadripod sidelobe. This agrees well with antenna gain patterns showing higher sidelobes generated by the quadripod structure.

E. Error Analysis

The noise temperature is determined from (1) the noise power measured with the power meter; and (2) the measured noise power and the noise temperature at both ambient load and zenith taken during calibration. The accuracy of the noise temperature measurement reported here therefore depends on the accuracy of calibration and of the power meter. Detailed analysis is given in the appendix. The result is the following upper bound for the standard deviation of the measurement of the noise temperature increase due to the sun:

for $T_{sn} \leq 2900$ kelvins,

$\sigma(T_{sn}) \leq 2.0 + 0.05\ T_{sn}$ kelvins

for $T_{sn} > 2900$ kelvins,

$\sigma(T_{sn}) \leq 2.0 + 0.15\ T_{sn}$ kelvins in the positive direction

$\leq 2.0 + 0.07\ T_{sn}$ kelvins in the negative direction

III. Predicted System Noise Temperature Increase Looking at the Center of the Sun

The expected increase in system noise temperature from a natural radio source is given as [3]

$$\Delta T = \frac{\eta S A}{2k} \tag{1}$$

where

η = 0.75 ± 0.05, antenna efficiency for the DSS 15 34-m antenna at 8420 MHz, looking at a source much larger than the beam solid angle. It includes the effect of spillover, blockage, VSWR, dissipation, and surface imperfection but does not include beam-broadening factors such as illumination, phase, and cross-polarization.

S = the flux density of the radio source, W/m^2-Hz

A = the physical area of the antenna, m^2

k = Boltzmann's constant (1.380622×10^{-23}), W/Hz-K

On the days of the measurements described here (November 26 and 27, 1987), the NOAA Space Environment Services Center[2] determined the total solar flux at 8800 MHz as measured at four locations over two days to be approximately

[2]U.S. Department of Commerce, National Oceanic and Atmospheric Administration, Environmental Research Laboratories, Space Environment Services Center, Boulder, Colorado.

259 Solar Flux Units, or SFUs (1 SFU = 1×10^{-22} watts/m^2-Hz), with a total spread in the measurement of about 50 SFUs. From comparisons of measurements made at a different time (February 3, 1988) at 4995 MHz and 8800 MHz, it was found that the solar flux varied with frequency approximately as

$$S \propto f^{1.2} \tag{2}$$

From this relationship, the flux at 8420 MHz (on November 26 and 27, 1987) is estimated to be

$$S = 246 \text{ SFUs}$$

The 1σ equivalent uncertainty of this estimate is about 5 percent, including the uncertainties of both steps.

The flux received by a narrow beam antenna is proportional to the ratio of the solid angle of the antenna to the solid angle of the solar disk. A number of corrections to this first-order approximation are discussed in [4]. The solid angle of the main beam is given by

$$\Omega_M = K_p \theta^2 \tag{3}$$

where

θ = the half-power beamwidth of the antenna main beam, measured at 0.061 degree for DSS 15 from 12-deg to 60-deg elevation by W. Wood (private communication); an uncertainty of 5 percent is estimated

K_p = a factor depending on pattern shape, estimated to be 1.03 ± 0.03 for nearly uniform illumination ([4], p. 221)

The solid angle of the sun is

$$\Omega_{sun} = \frac{\pi}{4} D^2 \tag{4}$$

where D is the diameter of the solar disk, or 0.533 degree.

Since the sun subtends an angle larger than the main beam, a correction to the main beam solid angle is made utilizing antenna pattern integrations made by T. Y. Otoshi (private communication). These calculations indicate that whereas 83.5 percent of the antenna power is in the main beam, 95.4 percent is within the solar disk. This correction is 14 percent. Therefore, the power within the solar disk is adjusted as follows:

$$\Omega'_M = 1.14\, \Omega_M \tag{5}$$

The noise temperature increase for the sun (at a 24-degree elevation angle where the antenna efficiency is 0.64) is then estimated to be

$$\Delta T = \frac{\eta S A}{2K} \cdot \left(\frac{\Omega'_M}{\Omega_{sun}} \right)$$

$$= 11{,}890 \text{ kelvins} \tag{6}$$

Finally, this estimate is corrected to include the effect of limb brightening [4], which is an increase in temperature at the edge of the solar disk. This increase is measured as a part of the total solar flux on the ground but is not observed by the main beam of the antenna, which is pointed to the center of the disk. This factor is estimated to be 0.99 ± 0.01. The estimated X-band temperature is therefore

$$\Delta T = 11{,}770 \text{ kelvins}$$

The uncertainty of this estimate is about 15 percent, calculated as the root of the sum of the squares of the individual percentage errors given above.

IV. Discussion

Figure 7 shows a comparison between the measured data and several data points taken during the Voyager solar conjunction at DSS 15 and DSS 43 using the standard DSN Noise Adding Radiometer. These points, with SEP angles greater than 0.5 degree, are seen to fall above and below the measured curve and hence are consistent with the measurement in this region. Therefore, the measurement can be used as a model for predicting the level of system temperature increase in this SEP range. Since the temperature is directly proportional to the solar flux density as explained in Section III, a prediction can be obtained by scaling the measured temperatures. The scale factor is simply the flux density at the time of interest divided by 246 SFUs, the flux density at 8.4 GHz during this measurement. The flux density at any given time can be roughly estimated according to the solar cycle.

The maximum measured noise temperature increase with the antenna pointing directly at the sun was about 8240 kelvins. However, the model described in the previous section estimates the solar noise temperature based on recorded solar flux to be 11,770 kelvins with an uncertainty of about 15 percent. Thus the measured temperature is 30 percent below the

prediction. The exact cause of this difference is unknown. One possibility is an unidentified nonlinearity in the receiver that has not been measured before. Table 1 suggests that this nonlinearity, if it exists, would have a significant effect only at temperatures above 2933 kelvins. Another possibility is error in the modeling.

V. Conclusion

System noise temperature increases at X-band due to the sun were measured at DSS 15, a 34-m HEF antenna, using the station open-loop receiver. The temperature was measured with an accuracy of about 5 percent up to 2900 kelvins. Temperatures above 2900 kelvins were adjusted to compensate for known nonlinearity in the receiving system. In this range the accuracy of the measurement is about 15 percent in the positive direction and 7 percent in the negative direction due to uncertainties in knowledge of the nonlinearity of the maser and the open-loop receiver.

The measurement agrees well with Voyager tracking data taken during the solar conjunction at SEP angles greater than 0.5 degree. It can be used as an experimental model for estimating system temperature increases for missions flying close to the sun, given a knowledge of the solar flux density at the desired time.

For temperatures obtained with the antenna pointing directly at the sun, there is a difference of 30 percent between the measured value of 8240 kelvins and the predicted value of 11,770 kelvins. The discrepancy in this extreme case is probably caused by unknown nonlinearities in the receiver, uncertainties in the model, or both.

As a result of the investigation, it has become evident that there is much uncertainty in the knowledge of the noise temperature of the solar disk and no proven prediction at angles off the disk. Further work is needed for the DSN to adequately characterize the noise temperature effects around the sun for the benefit of deep space missions.

Acknowledgments

The authors are grateful to M. Wert and R. Caswell of DSN Operations for their help in implementing the procedure and the power meter. R. Owen and V. Sutton were indispensable for their flawless operation of the antenna and equipment at Goldstone during the measurement. Thanks are especially due to C. Stelzried for providing helpful discussion in the preparation of this report.

References

[1] D. A. Bathker and D. W. Brown, "Large Ground Antenna Performance with Solar Noise Jamming," *Proceedings of the IEEE*, pp. 1949–1951 and 1966, December 1966.

[2] M. M. Franco, S. D. Slobin, and C. T. Stelzried, "20.7 and 31.4 GHz Solar Disk Temperature Measurements," *TDA Progress Report 42-64*, vol. May–June 1981, Jet Propulsion Laboratory, Pasadena, California, pp. 140–159, August 15, 1981.

[3] J. A. Turegano and M. J. Klein, "Calibration Radio Sources for Radio Astronomy: Precision Flux Density Measurements at 8420 MHz," *Astronomy and Astrophysics*, vol. 86, pp. 46–49, 1980.

[4] J. D. Kraus, *Radio Astronomy*, New York: McGraw-Hill, 1966.

[5] C. T. Stelzried, "Errors in Noise Temperature Measurement," *The Deep Space Network: Noise Temperature Concepts, Measurements, and Performance*, JPL Publication 82-33, Jet Propulsion Laboratory, Pasadena, California, pp. 25-1–25-3, September 15, 1982.

Table 1. Saturation of the Block IIA X-band maser at high noise power (maser gain set at 45 dB)

Noise power at maser input, kelvins	Maser gain compression, dB
736	0
2933	0.1
36,931	1.0
92,767	2.0

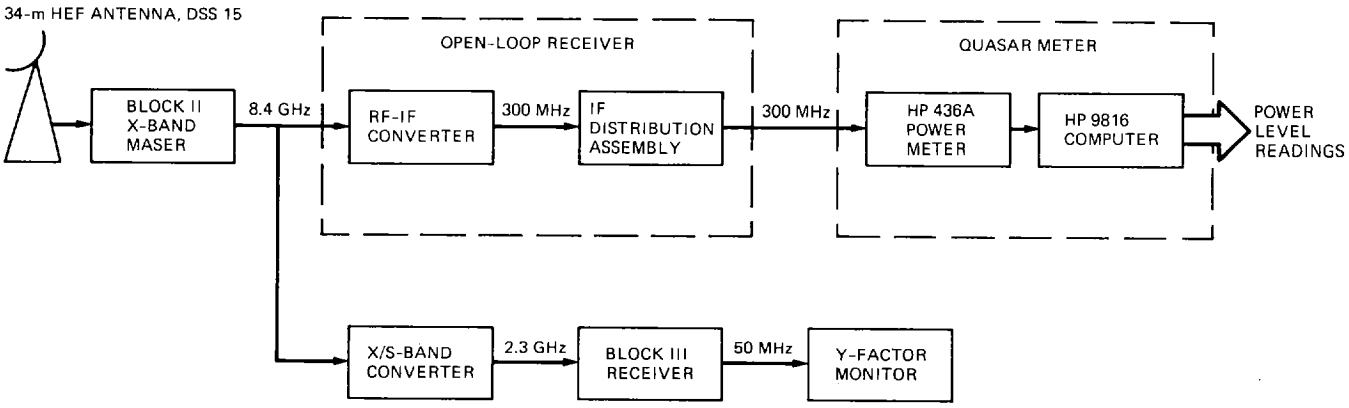

Fig. 1. Block diagram of the measurement system

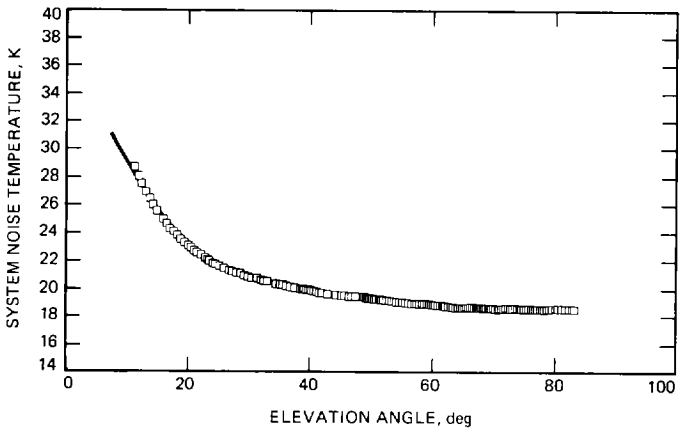

Fig. 2. DSS-15 34-meter HEF X-band system noise temperature (with atmosphere), measured on January 12, 1988

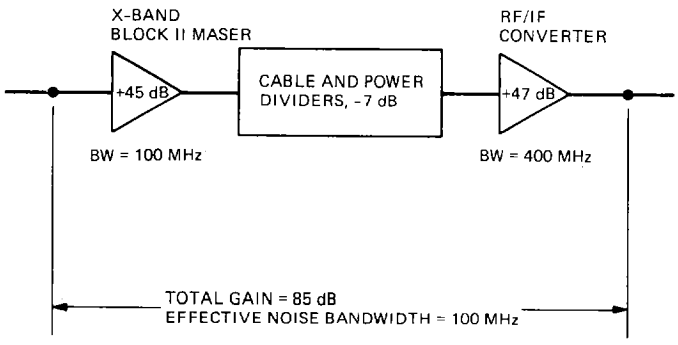

Fig. 3. Receiver gains and bandwidths for saturation analysis

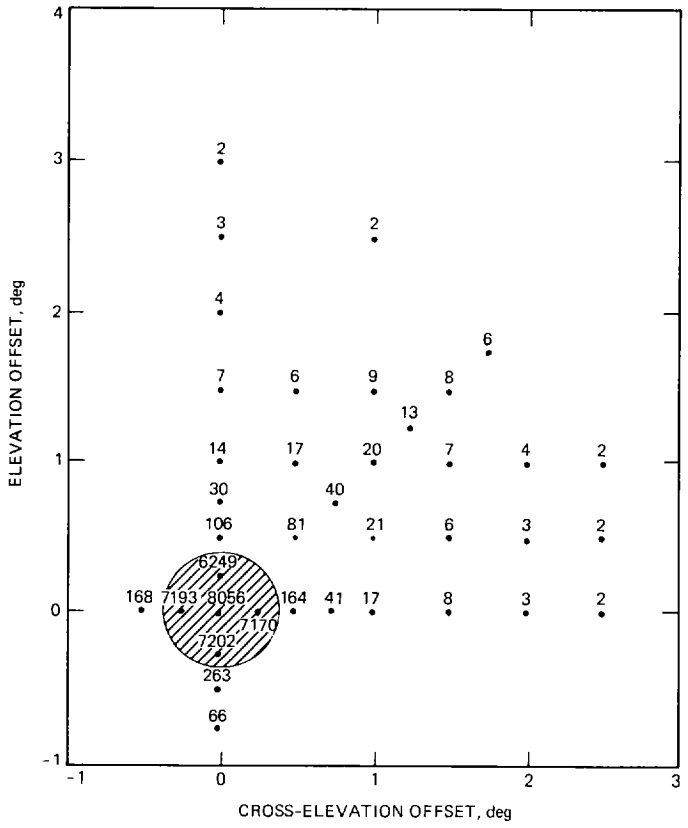

Fig. 4. System temperature increase due to the sun at angular offsets from the antenna boresight, measured on November 26, 1987. Numbers within the circle are below prediction due to unaccounted receiver nonlinearity or model errors.

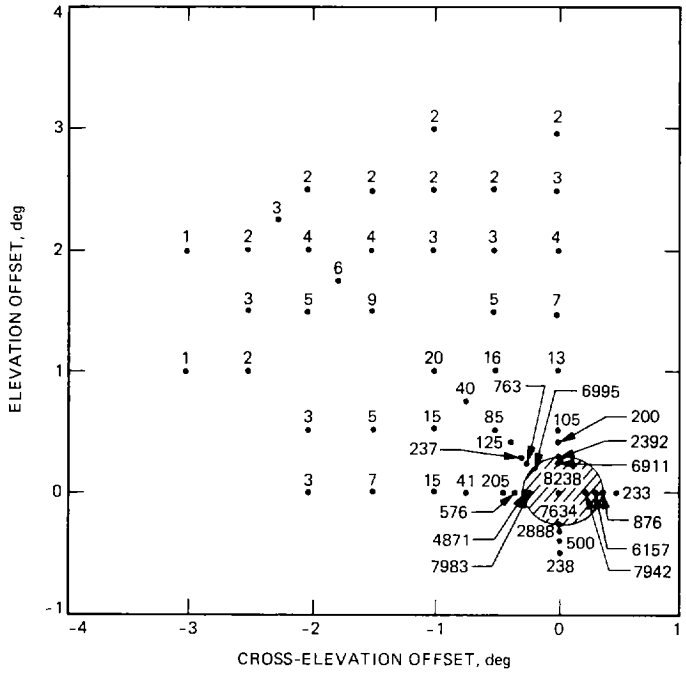

Fig. 5. System temperature increase due to the sun at angular offsets from the antenna boresight, measured on November 27, 1987. Numbers within the circle are below prediction due to unaccounted receiver nonlinearity or model errors.

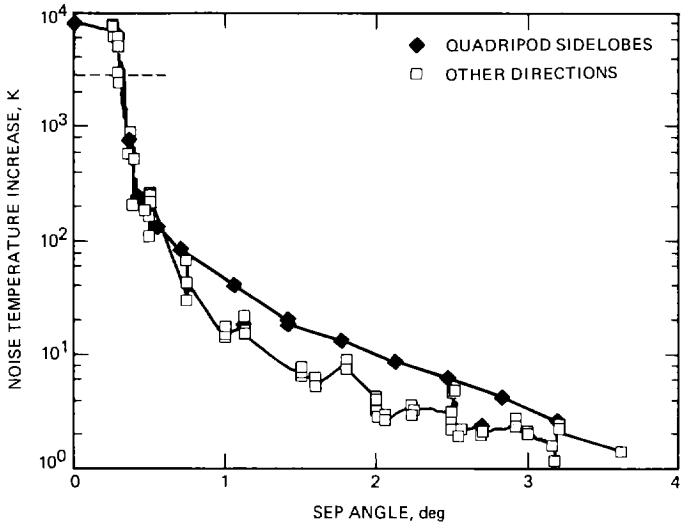

Fig. 6. System temperature increases due to the sun at various SEP angles, showing larger temperature increases along quadripod sidelobes. Data points above the dotted line are below prediction due to unaccounted receiver nonlinearity or model errors.

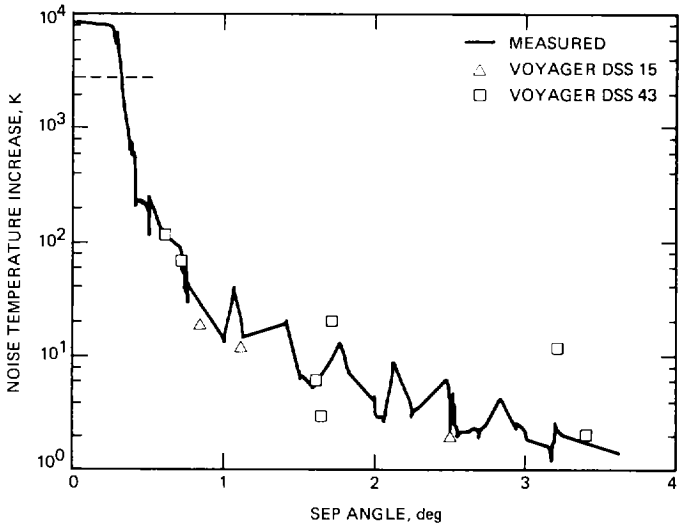

Fig. 7. Comparison of DSS-15 measured increase of system temperature with Voyager tracking data obtained at DSS 15 and DSS 43 during solar conjunction. Data points above the dotted line are below prediction due to unaccounted receiver nonlinearity or model errors.

Appendix

Calculating Error Bounds on Temperature Measurements

This appendix describes the method used to obtain estimates of error on the noise temperature measurements. The measured noise temperature (T_m) in all cases is derived from the relation

$$T_m = (P_m - P_s)(T_a - T_s)/(P_a - P_s) + T_s \qquad \text{(A-1)}$$

where P_m is the measured power, P_s is the power reading at cold sky, T_s is the sky temperature (measured using the Y-factor method), P_a is the power reading at ambient, and T_a is the ambient temperature. Note that P_s, T_s, P_a, and T_a were measured during calibration. For temperatures above 736 kelvins the power, P_m, is compensated for the maser saturation prior to applying Eq. (A-1).

Each parameter to the right of the equation is an average of many data points. Uncertainties in these parameters contribute to the uncertainty of the noise temperature. This is shown in the following equation obtained by taking differentials on both sides of Eq. (A-1):

$$\begin{aligned}\delta T_m = {} & \delta P_m (T_a - T_s)/(P_a - P_s) \\ & - \delta P_s [(T_a - T_s)/(P_a - P_s) \\ & + (P_m - P_s)(T_a - T_s)/(P_a - P_s)^2] \\ & + \delta P_a (P_m - P_s)(T_a - T_s)/(P_a - P_s)^2 \\ & + \delta T_a (P_m - P_s)(P_a - P_s) \\ & + \delta T_s [1 - (P_m - P_s)/(P_a - P_s)] \end{aligned} \qquad \text{(A-2)}$$

Expressing $P_m - P_s$ in terms of $T_m - T_s$ according to Eq. (A-1) and rearranging terms in Eq. (A-2), we have the following equation:

$$\begin{aligned}\delta T_m = {} & \delta T_s + (\delta P_m - \delta P_s)(T_a - T_s)/(P_a - P_s) \\ & + (T_m - T_s)[(\delta T_a - \delta T_s)/(T_a - T_s) \\ & - (\delta P_a - \delta P_s)/(P_a - P_s)] \end{aligned} \qquad \text{(A-3)}$$

The first term on the right is the error in calibrating the reference noise temperature. The second term is the effect of error in the power meter reading when an actual measurement is taken. Finally, the third term represents an error which is linearly increasing with the noise temperature measured. The slope of the increase is determined by calibration errors.

It can be shown that the standard deviation of the sum of several quantities is bounded from above by the sum of the standard deviations of the individual quantities. We now use this inequality on Eq. (A-3) to establish an upper bound on the temperature error:

$$\begin{aligned}\sigma(T_m) \leqslant {} & \sigma(T_s) + \sigma(P_m - P_s)(T_a - T_s)/(P_a - P_s) \\ & + (T_m - T_s)[\sigma(T_a - T_s)/(T_a - T_s) \\ & - \sigma(P_a - P_s)/(P_a - P_s)] \end{aligned} \qquad \text{(A-4)}$$

An upper bound of the standard deviation of each term on the right hand side is estimated below [5]:

$$\sigma(T_s) \leqslant 0.7 \text{ kelvin}$$

$$\begin{aligned}\sigma(P_m - P_s) &\leqslant \sigma(P_m) + \sigma(P_s) \\ &\leqslant 0.02P_m + 0.02P_s\end{aligned}$$

The inequality above is based on the power meter specification and the observed noise in measured data, to an effective one-sigma uncertainty of 2 percent. It can be rewritten as:

$$\sigma(P_m - P_s) \leqslant 0.02(P_m - P_s) + 0.04P_s$$

Using this inequality and Eq. (A-1) we obtain

$$\begin{aligned}\sigma(P_m - P_s)(T_a - T_s)/(P_a - P_s) &\leqslant 0.02(T_m - T_s) \\ &\quad + 0.04P_s(T_a - T_s)/(P_a - P_s) \\ &\leqslant 0.02(T_m - T_s) + 0.8\end{aligned}$$

The last inequality uses the approximate values of T_a (300 kelvins), T_s (19 kelvins), and the ratio of P_a to P_s of approximately 15.

$$\begin{aligned}\sigma(T_a - T_s)/(T_a - T_s) &\leqslant [\sigma(T_a) + \sigma(T_s)]/(T_a - T_s) \\ &\leqslant 0.004\end{aligned}$$

The last inequality uses the estimates $\sigma(T_a) \leq 0.4$ kelvin and $\sigma(T_s) \leq 0.7$ kelvin after Stelzried [5].

$$\sigma(P_a - P_s)/(P_a - P_s) \leq [\sigma(P_a) + \sigma(P_s)]/(P_a - P_s)$$

$$\leq [0.02P_a + 0.02P_s]/(P_a - P_s)$$

$$\leq 0.023$$

The last inequality uses the approximate ratio of P_a to P_s, 15, as before.

Summarizing the above, we arrive at the following:

$$\sigma(T_m) \leq 0.7 + 0.8 + (T_m - T_s)(0.02 + 0.004 + 0.023) \text{ kelvins}$$

With $T_s = 19$ kelvins, we have

$$\sigma(T_m) \leq 1.5 + 0.05(T_m - 19) \text{ kelvins}$$

This is a compact inequality showing the error in measured temperature as a function of the temperature. However, the temperatures plotted in Figs. 4–7 are actually the solar noise temperatures (T_{sn}):

$$T_{sn} = T_m - T_{\text{elev}}$$

where T_{elev} is the system noise temperature as a function of elevation angle (shown in Fig. 2) removed to normalize the measurements to solar effects only. Assuming that no additional error enters from T_{elev}, we have:

$$\sigma(T_{sn}) \leq 1.5 + 0.05(T_{sn} + T_{\text{elev}} - 19) \text{ kelvins}$$

At most, T_{elev} is about 30 kelvins. This gives

$$\sigma(T_{sn}) \leq 2.0 + 0.05 T_{sn} \text{ kelvins}$$

One final consideration lies in the maser noise saturation for very high noise temperatures. When the measured noise temperature is above 2900 kelvins, the nonlinearity of the Block II X-band maser is compensated. This compensation could be off by a maximum of about 10 percent in the positive direction and 2 percent in the negative direction as mentioned in Section IIE. These errors are added to the error when temperatures exceed 2900 kelvins. In summary, the standard deviation of the error in the solar noise temperature is as follows:

for $T_{sn} \leq 2900$ kelvins,

$\sigma(T_{sn}) \leq 2.0 + 0.05\ T_{sn}$

for $T_{sn} > 2900$ kelvins,

$\sigma(T_{sn}) \leq 2.0 + 0.15\ T_{sn}$ kelvins in the positive direction

$\leq 2.0 + 0.07\ T_{sn}$ kelvins in the negative direction